HHS Public Access

Author manuscript

Metall Mater Trans A Phys Metall Mater Sci. Author manuscript; available in PMC 2021 June 29.

Published in final edited form as:

Metall Mater Trans A Phys Metall Mater Sci. 2020 September ; 51(9): 4406–4413. doi:10.1007/s11661-020-05878-y.

Highly Ductile Zn-2Fe-WC Nanocomposite as Biodegradable Material

Zeyi Guan[a], **Chase S. Linsley**[b], **Shuaihang Pan**[a], **Christina DeBenedetto**[b], **Jingke Liu**[a], **Benjamin M. Wu**[b,c,d,e], **Xiaochun Li**[a,c,*]

[a]Department of Mechanical & Aerospace Engineering, Samueli School of Engineering, University of California, Los Angeles, CA, USA

[b]Department of Bioengineering, Samueli School of Engineering, University of California, Los Angeles, CA, USA

[c]Department of Materials Science & Engineering, Samueli School of Engineering, University of California, Los Angeles, Los Angeles, CA, USA

[d]Division of Advanced Prosthodontics, School of Dentistry, University of California, Los Angeles, CA, USA

[e]Department of Orthopedic Surgery, David Geffen School of Medicine, University of California, Los Angeles, CA, USA

Abstract

Zinc (Zn) has been widely investigated as a biodegradable metal for orthopedic implants and vascular stents due to its ideal corrosion in vivo and biocompatibility. However, pure Zn lacks adequate mechanical properties for load-bearing applications. Alloying elements, such as iron (Fe), have been shown to improve the strength significantly, but at the cost of compromised ductility and corrosion rate. In this study, tungsten carbide (WC) nanoparticles were incorporated into the Zn-2Fe alloy system for strengthening, microstructure modification, and ductility enhancement. Thermally stable WC nanoparticles modified the intermetallic ζ-$FeZn_{13}$ interface morphology from faceted to non-faceted. Consequently, WC nanoparticles simultaneously enhance mechanical strength and ductility while maintaining a reasonable corrosion rate. Overall, this novel Zn-Fe-WC nanocomposite could be used as biodegradable material for biomedical applications where pure Zn is inadequate.

INTRODUCTION

Zn and its alloys have been proposed and intensively studied in the last decade as an innovative candidate for degradable biomedical implants, especially as bioresorbable cardiovascular stents. Compared with magnesium and its alloys, which have been comprehensively studied as biodegradable materials for more than 20 years,[1] Zn alloys offer excellent biocompatibility in addition to a tolerable bio-corrosion rate.[2] The relatively slow degradation process of Zn causes no aggressive hydrogen bubble evolution

*corresponding author.

when comparing to Mg.[3] Furthermore, Zn and its alloys exhibited excellent ductility, where hot extruded pure Zn wire achieved greater than 70 pct elongation before failure.[4] Finally, Zn is highly compatible with the human body as it is the second most abundant transition metal in the human body.[5] However, newly developed biodegradable Zn medical implants are limited to non-loading bearing applications because Zn has limited mechanical strength.[6] Alloying is commonly used to strengthen materials, and several Zn alloys have been studied to obtain the desired combination of mechanical and biological properties required for use as degradable implant materials.[7] However, the selection of alloying elements is extremely limited because the metal ions leached during the degradation process must not cause a chronic inflammatory response. Additionally, any alloying element that promotes a high concentration of intermetallic precipitate could compromise the corrosion rate and ductility.

Zn-Fe alloys serve as potential candidates that could provide strengthening while retaining excellent biocompatibility.[8,9] The alloying element Fe has been evaluated as degradable material that can degrade in the physiological environments with little-to-no inflammatory response.[10] A low concentration of Fe in as-cast Zn has been shown to provide efficient precipitation strengthening, reaching more than 130 MPa in ultimate tensile strength (UTS). Additionally, Zn-Fe alloy showed little sign of anemia from in vivo assessment, and the corrosion rate remained 13 μm/year, within the maximum corrosion rate requirement of 20 μm/year.[11,12] However, the lack of ductility remains one of the critical limitations of the Zn-Fe alloy system, due to the formation of brittle ξ phase ($FeZn_{13}$). Previous studies proposed using less than 0.3 wt pct Al to suppress brittleness by inhibiting the formation of ξ phase in the Zn-Fe alloys.[13,14] However, chronic exposure to Al can have cytotoxic effects in animals and is not suitable for such biomedical applications.[15]

This work provides a novel method using WC nanoparticles as dispersed phases to modify the morphology of the brittle, faceted Zn-Fe intermetallic phase. The primary purpose of nanoparticles is to enhance the mechanical strength through Orowan strengthening and to modify the ξ phase formation and growth by serving as nucleation sites and grain growth blockers to control the intermetallic microstructure and morphology.[16] These intermetallic phases changed to non-faceted morphology to avoid crack initiation, enabling effective dislocation pinning, and simultaneously increasing the strength and ductility.[17] Meanwhile, compared with the Al alloying element, chemically stable WC nanoparticles are generally inert and non-reactive in the human body with no W ion leaching. Moreover, WC nanoparticles show no acute toxicity to mammalian cell lines.[18] These aforementioned facts reasonably imply the biocompatibility of Zn-Fe-WC nanocomposite for biodegradable metallic implants.

MATERIALS AND METHODS

Salt assisted stir casting and ultrasound processing were performed to manufacture the Zn-WC nanocomposite, shown in Figure 1. An induction furnace was used to melt potassium aluminum fluoride ($KAlF_4$) at 800 °C in a graphite crucible. Bulk Zn pellets (99.9 pct, RotoMetals) were weighed and added to the crucible. WC nanoparticles (150 nm diameter on average) were mixed with fine $KAlF_4$ salt powders at a volume ratio of 1:20. This powder

mixture was gradually added to the crucible until 8 vol pct WC nanoparticles concentration in Zn was reached. A graphite stirrer was used to mix and effectively incorporate WC nanoparticles (500 rpm, 1.0 hour). Ultrasound processor (Misonix S-400 Ultrasonic Liquid Processor, Nb probe) was used to further homogeneously dispersed the nanoparticles and eliminate molten salt that was trapped in the metal melt. Granular Fe metal pieces (Alfa Aesar, 20 mesh, 99 pct) were weighed and added to the crucible. The temperature was maintained at 800 °C for 20 minutes, and the metal melt was cast to steel mold. Zn-2Fe-WC samples were post-processed with hot rolling under a thickness reduction of 10:1 at 250 °C. Wire-electrical discharge machining (wire-EDM) was used to cut samples to dog-bone shape for the tensile test (ASTM E8/E8M standard sub-size). Tensile tests were carried out using Instron ElectroPlus 1000 mechanical tester at a strain rate of 2 mm/min. 0.2 pct proof stress was used as yield strength.

Grain etchant (20 g CrO_3, 5 g Na_2SO_4) was applied as an etchant to expose the intermetallic phase for optical microscopy imaging (Zeiss Primotech optical microscopy). Microhardness test was performed by LM 800AT microhardness tester using a load of 200 gf with a 10 seconds dwell time. The as-cast high purity Zn-2Fe and as-cast Zn-2Fe-8 vol pct WC nanocomposites were prepared by mechanical grinding, alumina nanoparticle polishing and ion milling polishing for microstructure characterization by scanning electron microscopy (ZEISS Supra 40VP SEM), energy-dispersive X-ray spectroscopy (EDS) and element detection by X-ray diffraction (XRD).

Electrochemical characterization was carried out with a VersaSTAT 4 (Ametek) using a three-electrode cell, which included a saturated calomel reference electrode (SCE), a graphite counter electrode and the specimen as the working electrode. The electrolyte was Hank's balanced salt solution (HBSS, Gibco) at pH 7.4. Tests were run at both room (23 °C) and body (37 °C) temperature. Puratronic® Zn wire (99.994 pct, 0.5 mm dia, Alfa Aesar), which has been swaged and cold drawn down to size, was used as received for the pure Zn specimen. Prior to electrochemical testing, each specimen was mechanically polished with SiC abrasive papers down to 1200 grit. The surfaces were cleaned in acetone within an ultrasound bath for 10 minutes, followed by nanopure water for 10 minutes. Before starting the potential scan, the open circuit potential (OCP) was measured for 1 hour as the specimen stabilized. The potential scan range for linear polarization resistance (LPR) was ± 20 mV from the stabilized OCP at a scan rate of 0.166 mV/s. The Tafel polarization scan range was ± 250 mV from the stabilized OCP at a scan rate of 0.166 mV/s. Corrosion rates based on electrochemical data were calculated according to ASTM-G102.

Immersion tests were carried out in HBSS (pH 7.4) at 37 °C. The ratio of surface area to volume was < 0.01 cm^2/mL. After immersion for 1, 3, 5, 7, 11, 14, 19, 22 and 28 days, aliquots of the immersion medium were collected, and fresh immersion medium was added to mimic sink conditions. The ion concentrations of Zn, Fe, and W in solution were detected using an inductively coupled plasma-mass spectrometry (ICP-MS, PerkinElmer).

RESULTS AND DISCUSSION

The typical microstructures of Zn-2Fe-WC were shown in Figure 2. Zn-2Fe-8 vol pct WC sample was observed from the SEM before etching, shown in Figure 2(a). Darker phases were the metal matrix, while brighter phases represented the nanoparticle formed pseudo-clusters. A higher magnification SEM image showed the good dispersion of WC nanoparticles within this pseudo-clusters in Figure 2(b). Such a phenomenon was reasonable due to the nanoparticle size effect and wettability between the WC nanoparticles and the molten Zn. Furthermore, an etched sample also showed the nanoparticle dispersion in the Zn-rich phase, but none in the ζ precipitates, shown in Figure 2(c). Point scannings were performed in different places to indicate that WC nanoparticles preferred to stay in the Zn-rich phase, shown in Figure 2(d). An EDX map scanning has indicated a total WC concentration of 8 vol pct for typical nanocomposite samples.

To further analyze the microstructure modification of Zn-Fe by dispersed WC nanoparticles during the solidification process, optical microscopy images were used to illustrate the microstructure of the intermetallics, as shown in Figure 3. Since Fe is not soluble in Zn at temperatures below 800 K, ζ precipitates are likely to form during the solidification process and be dispersed homogeneously across the bulk alloy.[11] Due to the non-uniform energy at different atomic orientation, the ζ phase had faceted morphology, as shown in Figures 3(a) and (b). Intermetallic phases commonly grow along the low energy surface, also known as the faceted interface.[19] These faceted interfaces can result in embrittlement and low elongation to failure, which has been demonstrated in Cu.[20] The Zn-2Fe-WC sample has a significantly different microstructure, shown in Figures 3(c) and (d). The ζ intermetallic, though grew in the zinc nanocomposite matrix with an average grain size similar to the reference samples, has non-faceted interfaces with Zn grains. It is believed that the well-dispersed nanoparticles in molten metal could effectively modify the faceted interface morphology to non-faceted ones during solidification.

According to the Zn-Fe phase diagram and the fact that nanoparticles rarely existed in the ξ phases, the interaction between WC nanoparticles and the molten metal during the solidification process can be deduced as following stages, shown in Figure 4:

1. WC nanoparticles were well-dispersed in metal zinc before cooling, partially due to the good wettability between molten zinc and WC.[21]
2. Nanoparticles initiated the intermetallic phase formation as nucleation sites. They also restricted the solidification front and modified the morphology of the ξ phase.[16]
3. Zinc matrix solidified as WC nanoparticles dispersed uniformly inside the matrix.

Chemical compositions of the samples were further confirmed through XRD, which detected both samples from 30 to 50 deg, shown in Figure 5. The intermetallic phases were confirmed to be ξ phase.

Vickers microhardness of as-cast Zn-2Fe and as-cast Zn-2Fe-WC was characterized using a microhardness tester compared with the pure Zn cast in the same method, shown in Figure 6. 8 vol pct WC nanoparticles primarily existed inside the zinc matrix, enabling the nanoparticle-induced precipitation strengthening.[21] WC nanoparticles with Vickers microhardness larger than 2200HV dispersed inside the material could efficiently impede the dislocation movement to enhance mechanical strength. Thus, in addition to the ξ phase hardening, WC nanoparticles further increase the Vickers microhardness from 47.9 to 59.3 HV.

Tensile testing was performed on Zn-2Fe and Zn-2Fe-WC, and the results are shown in Figure 7. With 8 vol pct WC nanoparticles, the ultimate tensile stress (UTS) and elongation to failure increased from 92.0 to 121.1 MPa and from 1.4 to 8.6 pct, respectively. The corresponding fracture surfaces of the specimens are shown in Figure 8. The pure Zn-2Fe sample has a flat fracture surface due to the brittleness of the zeta phase. In contrast, Zn-2Fe-WC had a large amount of WC nanoparticles on the fracture surface, which potentially impedes the propagation of cracks. To further improve the nanocomposite material's mechanical behavior, the hot rolling process was performed on Zn-2Fe-WC. The results showed that the UTS and elongation to failure increased to 155.8 MPa and 15.3 pct. The improved performance of the hot-rolled (HR) sample suggests a reduction in porosity and improvement in nanoparticle dispersion,[22] which enhances both ductility and strength. [23]

The tensile test data of as-cast Zn-2Fe-WC samples showed a significant ductility improvement, compared with other biodegradable Zn alloys, whose alloying elements include Mg, Ca, Fe, and Sr, as shown in Figure 9. With the addition of WC nanoparticles that homogeneously modified the strengthening intermetallic phases, the elongation to failure of Zn-2Fe reached more than 8 pct, exceeding most of the as-cast Zn alloys. The non-faceted morphology of the intermetallic phase is presumed to be the critical factor in improving the ductility. Although the Zn-2Fe-WC did not offer a relatively high strength suitable for load-bearing biodegradable implants such as bone plates and cardiovascular stents, this work has shown an effective method to improve ductility for as-cast zinc alloys, providing a solution for the manufacturing of ductile biodegradable Zn alloys. In the previous work, hot work processing (e.g., hot extrusion and hot rolling) was a necessary procedure to gain ductility due to the HCP atomic structure of Zn. Such processes limited the manufacturing of complex geometries. Laser micromachining was introduced to solve this problem, but the heat affected zone is a side effect for most commercially available lasers. Thus, this work leveraged the simple casting method for Zn and Zn alloy, which has no geometry restriction and could further broaden the applications of Zn alloys.

One of the reasons Zn has been extensively studied as a biodegradable implant material is its suitable corrosion rate for many biomedical applications, but the addition of alloy elements have been shown to deteriorate this property. The corrosion resistance of the as-cast Zn, Zn-2Fe, and Zn-2Fe-WC was evaluated by electrochemical analysis.[24] The corrosion rate was calculated from Eq. [1]

$$CR = 3.27 \cdot 10^{-3}(i_{corr}EW/\rho) \quad (1)$$

where CR is the corrosion rate (mm/year), i_{corr} is the corrosion current density (uA/cm^2), EW is the equivalent weight of the metal, and ρ is the density (g/cm^3). No difference in the CR was measured between as-cast Zn, Zn-2Fe, and Zn-2Fe-WC, shown in Table I. It has been previously reported that Zn-Fe alloys have greater corrosion rates compared to pure Zn due to ξ phase acting as a cathode to the Zn matrix, causing accelerated degradation by microgalvanic effect.[11] Since electrochemical techniques capture the corrosion behavior of a specimen during the narrow window of time over which the measurement was carried out, immersion tests were also carried out to investigate corrosion behavior (Table II and Figure 10). In the first week, Zn ion release was the greatest from the samples alloyed with Fe, and the Zn-2Fe samples had the greatest followed by Zn-2Fe-WC; however, by day 14, there was no difference in the cumulative Zn ion release between the 3 different groups. Similarly, the release of Fe from the Zn-2Fe samples was greater than the samples containing the WC nanoparticles in the first 2 weeks, but there was no difference in cumulative Fe ion release after day 14. These results corroborate the electrochemical testing, which found no difference in CR between the pure Zn and the samples alloyed with 2 wt pct Fe and 8 vol pct WC nanoparticles. Long-term immersion studies (i.e., 3 + months) and in vivo studies are required to elucidate the corrosion behavior of Zn-Fe based nanocomposites and their applicability as a biodegradable implant material. Encouragingly, little-to-no W ions were released after 28 days. Only one sample had measurable levels of W ions, and by day 28, the cumulative release was 2 ng/mm2. For elemental W to be detectable, the WC nanoparticles must first escape the bulk metal and undergo oxidation to release W ions. For biomedical applications, it is more likely that cells will encounter WC nanoparticles over elemental W, and both cytotoxicity and genotoxicity of WC nanoparticles on relevant cell lines are required.

CONCLUSION

A Zn-Fe based nanocomposite with WC nanoparticles was successfully manufactured using molten salt-assisted stir casting and ultrasound processing. With 8 vol pct WC, as-cast Zn-2Fe had improved ductility from 1.4 to 8.6 pct, while maintaining high mechanical strength. The WC nanoparticles introduced phase control by blocking the intermetallic ζ-phase growth during the solidification process, which transform the faceted intermetallic morphology to non-faceted. This phenomenon resulted in significantly enhanced ductility during tensile properties characterization. The electrochemical test and immersion tests verified that the suitable corrosion rate of Zn-2Fe was not impacted by the alloying element and the WC nanoparticles, which further supports the continued study of Zn-2Fe-WC as biodegradable material for medical applications. In conclusion, this work has broadened the application of Zn-Fe alloy by incorporating nanoparticles to obtain a combination of high strength, high ductility, and modest corrosion rate.

ACKNOWLEDGMENTS

The research reported in this publication was supported by the National Heart, Lung, And Blood Institute of the National Institutes of Health under Award Number R01HL143465. The content is solely the responsibility of the authors and does not necessarily represent the official views of the National Institutes of Health.

REFERENCES

1. Heiden M, Walker E and Stanciu L: J. Biotechnol. Biomater, 2015, vol. 5, pp. 1–9.
2. Bowen PK, Drelich J and Goldman J: Adv. Mater, 2013, vol. 25, pp. 2577–82. [PubMed: 23495090]
3. Thomas S, Medhekar NV, Frankel GS and Birbilis N: Curr. Opin. Solid. State. Mater. Sci, 2015, vol. 19, pp. 85–94.
4. Mostaed E, Sikora-Jasinska M, Mostaed A, Loffredo S, Demir A, Previtali B, Mantovani D, Beanland R and Vedani M: J. Mech. Behav. Biomed, 2016, vol. 60, pp. 581–602.
5. Mostaed E, Sikora-Jasinska M, Drelich JW and Vedani M: Acta. Biomater, 2018, vol. 71, pp. 1–23. [PubMed: 29530821]
6. Liu X, Sun J, Yang Y, Pu Z and Zheng Y: Mater. Lett, 2015, vol. 161, pp. 53–56.
7. Bowen PK, Shearier ER, Zhao S, Guillory RJ, Zhao F, Goldman J and Drelich JW: Adv. Healthc. Mater, 2016, vol. 5, pp. 1121–40. [PubMed: 27094868]
8. Liu B and Zheng Y: Acta. Biomater, 2011, vol. 7, pp. 1407–20. [PubMed: 21056126]
9. Vojtech D, Kubasek J, Capek J and Pospisilova I: Mater. Technol, 2015, vol. 49, pp. 877–82.
10. Waksman R, Pakala R, Baffour R, Seabron R, Hellinga D and Tio FO: J. Interv. Cardiol, 2008, vol. 21, pp. 15–20. [PubMed: 18086136]
11. Kafri A, Ovadia S, Goldman J, Drelich J and Aghion E: Metals, 2018, vol. 8, pp. 1–15.
12. Kafri A, Ovadia S, Yosafovich-Doitch G and Aghion E: J. Mater. Sci. Mater. Med, 2018, vol. 29, pp. 1–8.
13. Porter FC: Zinc handbook: properties, processing, and use in design. (CRC Press, Boca Raton, 1991).
14. Culcasi J, Sere P, Elsner C and Di Sarli A: Surf. Coat. Technol, 1999, vol. 122, pp. 21–23.
15. Jones DL and Kochian LV: FEBS. Lett, 1997, vol. 400, pp. 51–57. [PubMed: 9000512]
16. Cao, Yao G, Jiang L, Sokoluk M, Wang X, Ciston J, Javadi A, Guan Z, De Rosa I and Xie W: Sci. Adv, 2019, 5, 2398
17. Cheng S, Zhao Y, Zhu Y and Ma E: Acta. Mater, 2007, vol. 55, pp. 5822–32.
18. Bastian S, Busch W, Kühnel D, Springer A, Meißner T, Holke R, Scholz S, Iwe M, Pompe W and Gelinsky M: Environ. Health Perspect, 2009, vol. 117, pp. 530–36. [PubMed: 19440490]
19. Hamilton JC, Siegel DJ, Daruka I and Léonard F: Phy. Rev. Lett, 2003, vol. 90, art. no. 246102.
20. Sigle W, Ciiang L-S and Gusr W: Phil. Mag. A, 2002, vol. 82, pp. 1595–608.
21. Guan Z, Pan S, Linsley C and Li X: Procedia Manuf, 2019, vol. 34, pp. 247–51. [PubMed: 34007864]
22. Tjong SC: Adv. Eng. Mater, 2007, vol. 9, pp. 639–52.
23. Zhou D, Qiu F and Jiang Q: Mater. Sci. Eng. A, 2015, vol. 622, pp. 189–93.
24. Yang H, Jia B, Zhang Z, Qu X, Li G, Lin W, Zhu D, Dai K, and Zheng Y: Nat. Comm, 2020, vol. 11, pp. 1–16.

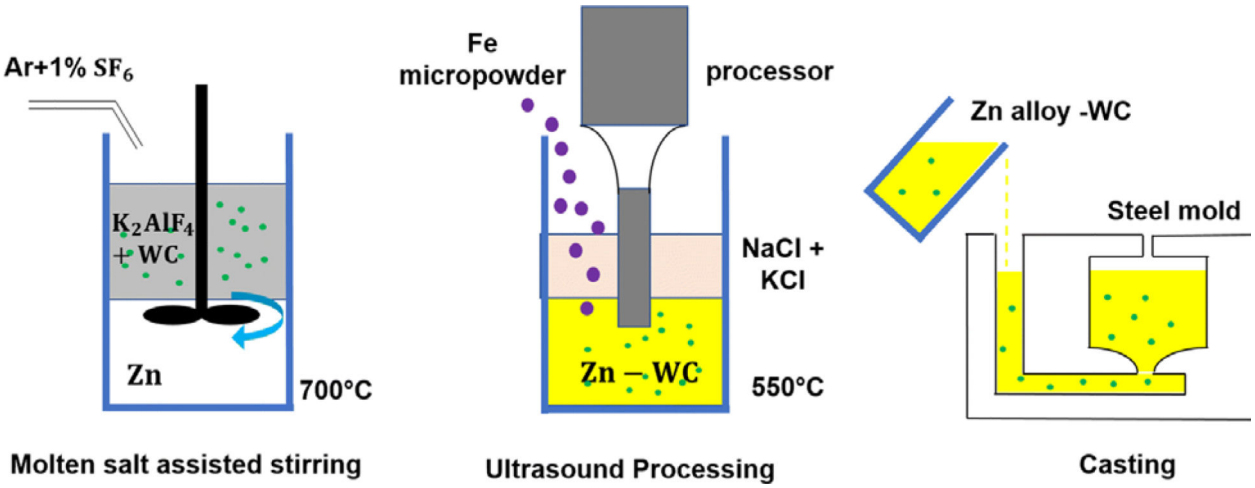

Fig. 1.
Schematics of Zn-Fe-WC nanocomposite manufacturing

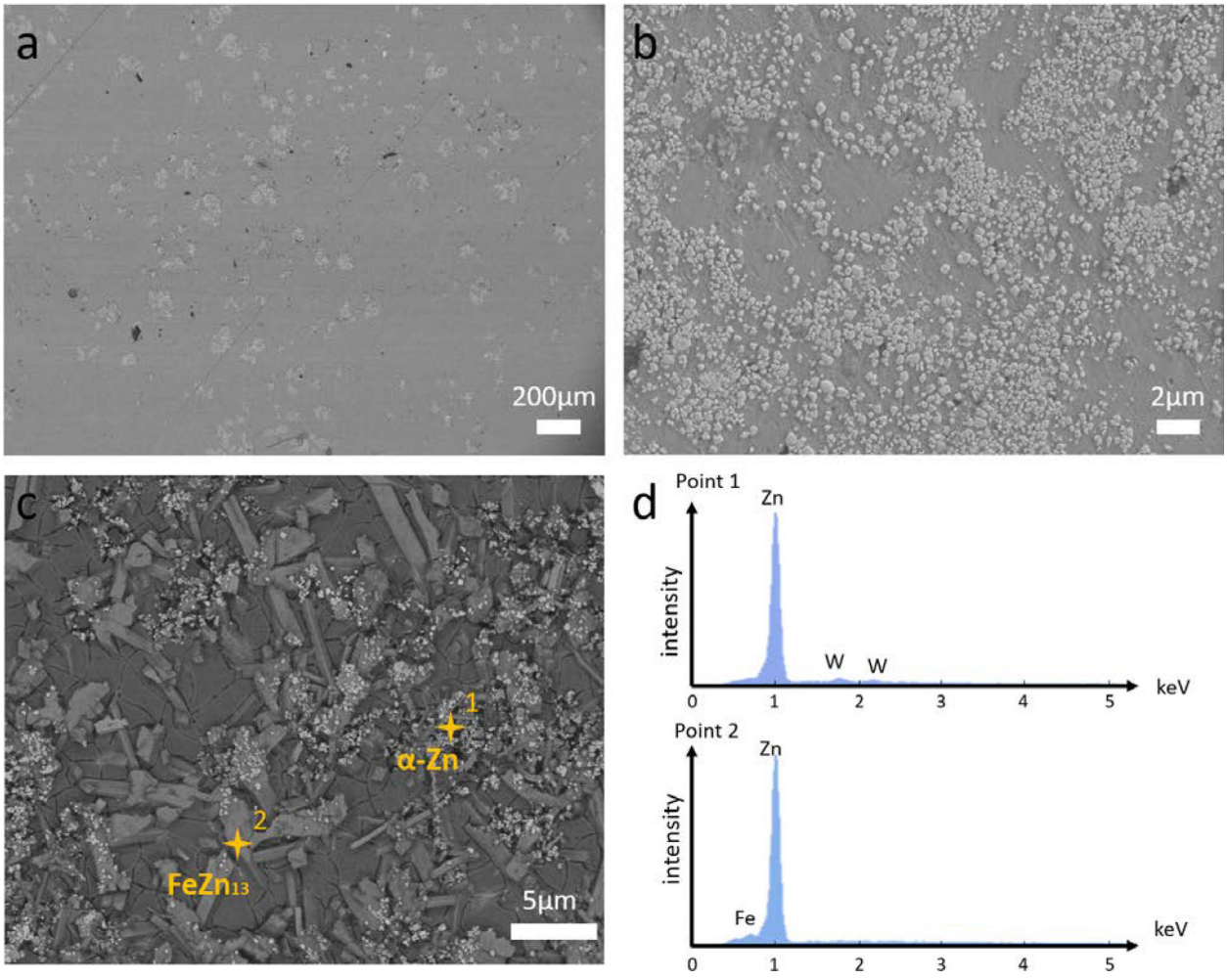

Fig. 2.

Microstructure of Zn-2Fe-8 vol pct WC. (*a*) The microstructure image of Zn-2Fe-WC under SEM at low magnification. Brighter phases indicated the high-density nanoparticle pseudo-clusters. (*b*) The microstructure image of Zn-2Fe-WC under SEM at high magnification, showing the good distribution of WC nanoparticles inside the pseudo-clusters. (*c*) SEM image of Zn-2Fe-WC after grain etching, showing nanoparticles modified the formation of $FeZn_{13}$. (*d*) EDS point scannings were performed on places shown in (c), indicating nanoparticles were likely to stay in Zn-rich phase

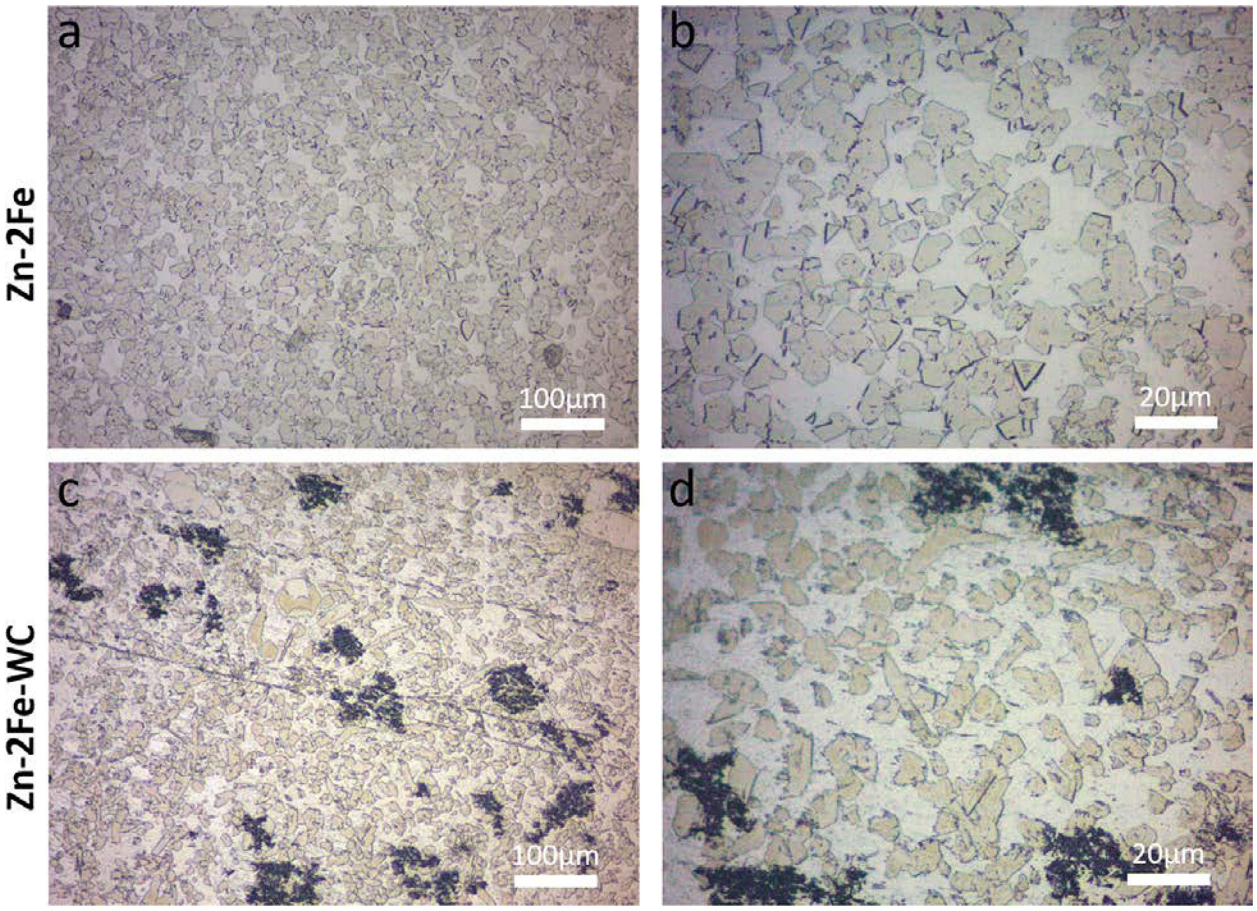

Fig. 3.

(*a*) and (*b*) Zn-2Fe optical images after etching, yellow phases indicated the faceted intermetallic precipitate (ζ-$FeZn_{13}$). (*c*) and (*d*) Zn-2Fe-WC optical images after etching, intermetallic phases showed non-faceted morphology and the black spots indicated the nanoparticle pseudo-clusters

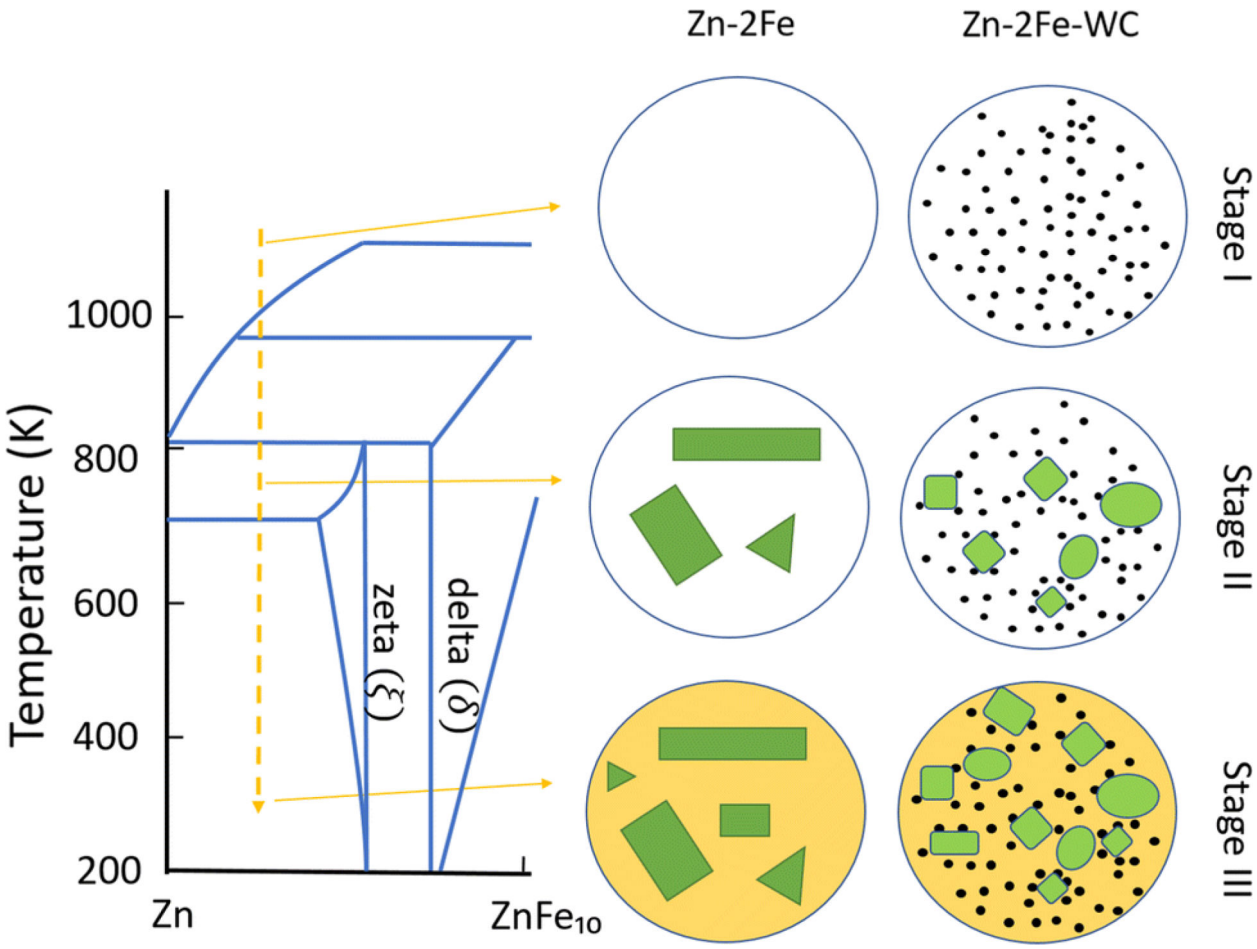

Fig. 4.
Proposed schematic of the solidification process for Zn-2Fe and Zn-2Fe-WC at stages I–III

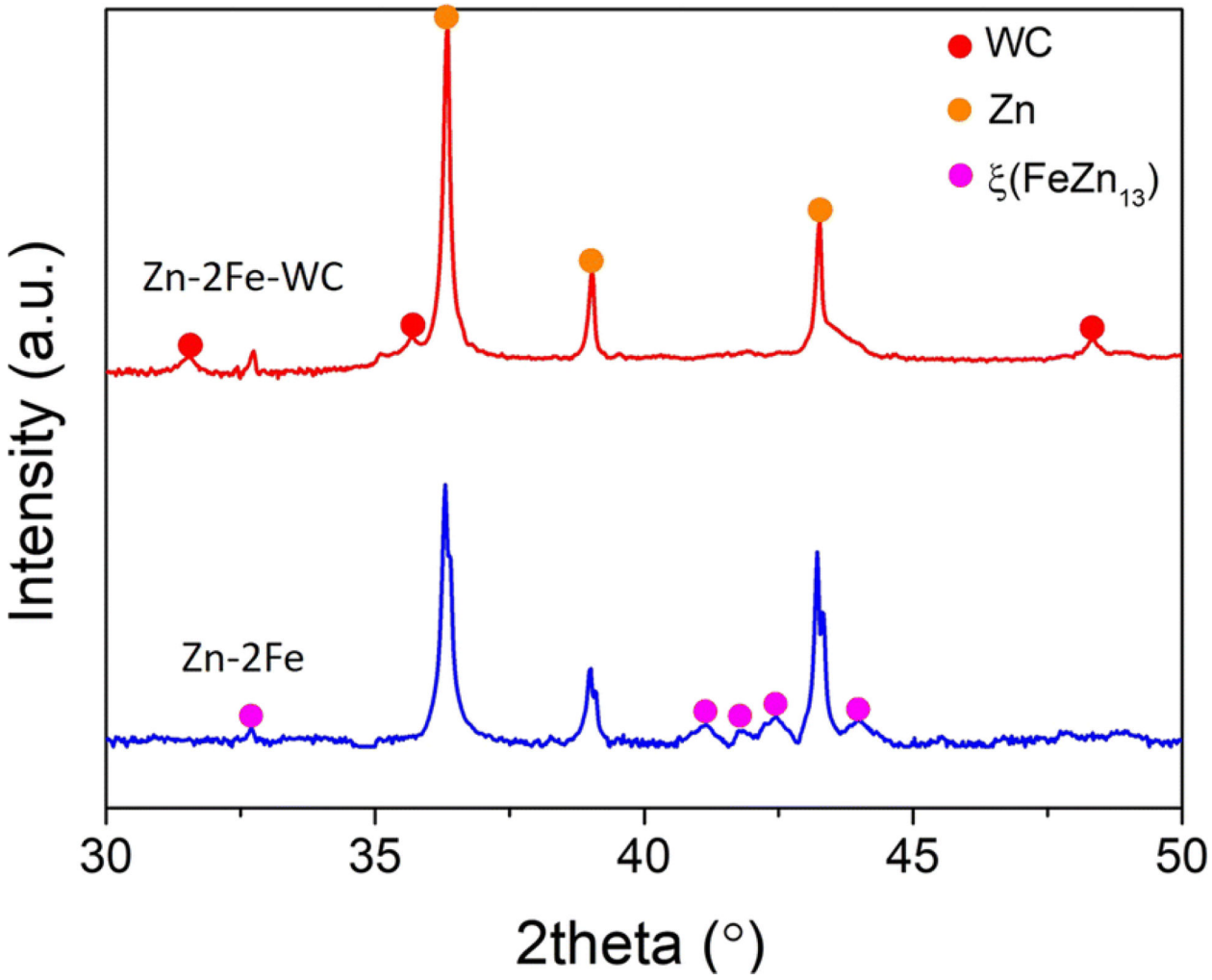

Fig. 5.
XRD results of Zn-2Fe and Zn-2Fe-WC

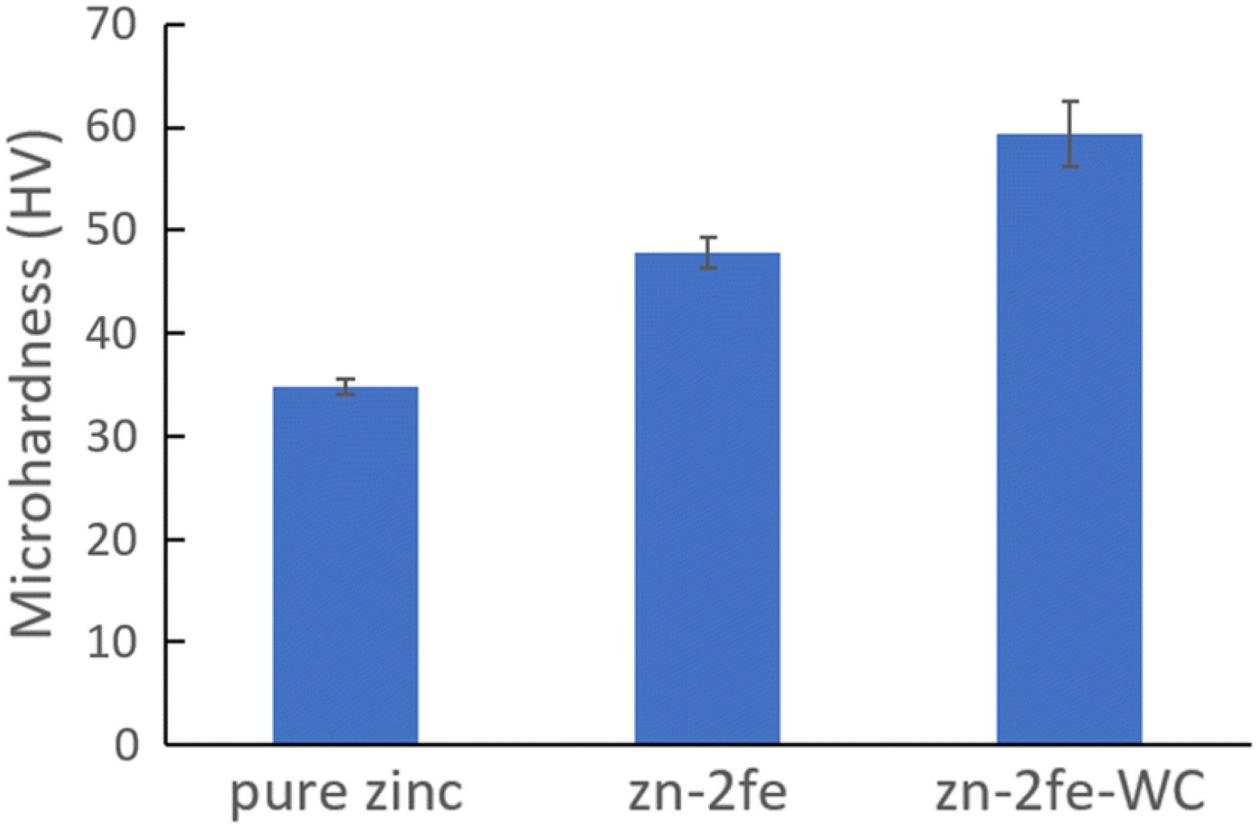

Fig. 6.
Vickers microhardness of Zn-2Fe and Zn-2Fe-WC compared with pure Zinc sample ($n = 8$)

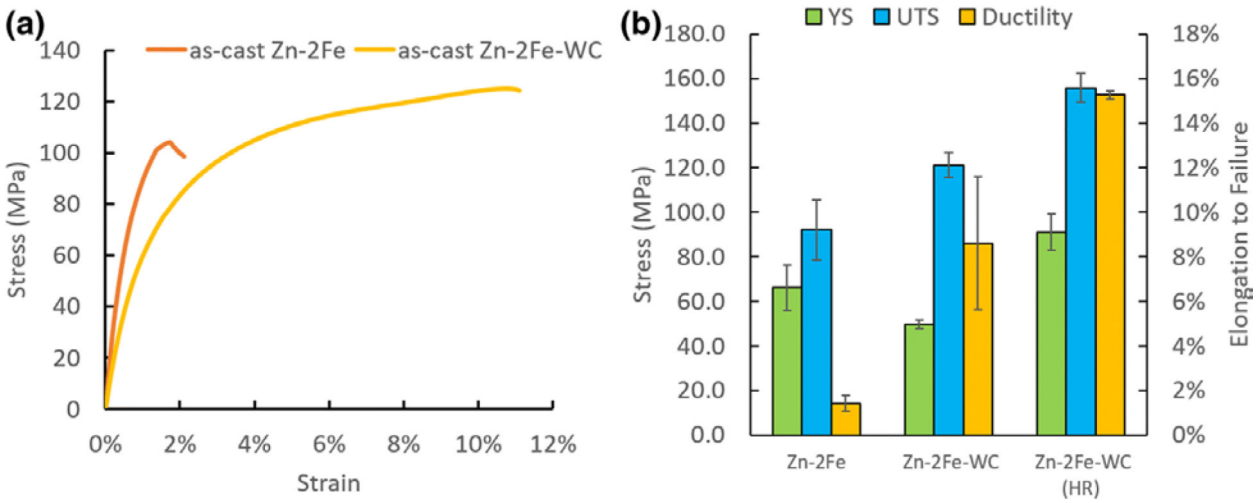

Fig. 7.

(*a*) Representative stress-strain curve from the tensile test of cast Zn-2Fe, cast Zn-2Fe-WC. (*b*) Average values of yield strength, ultimate tensile strength, and elongation to failure ($n = 3$)

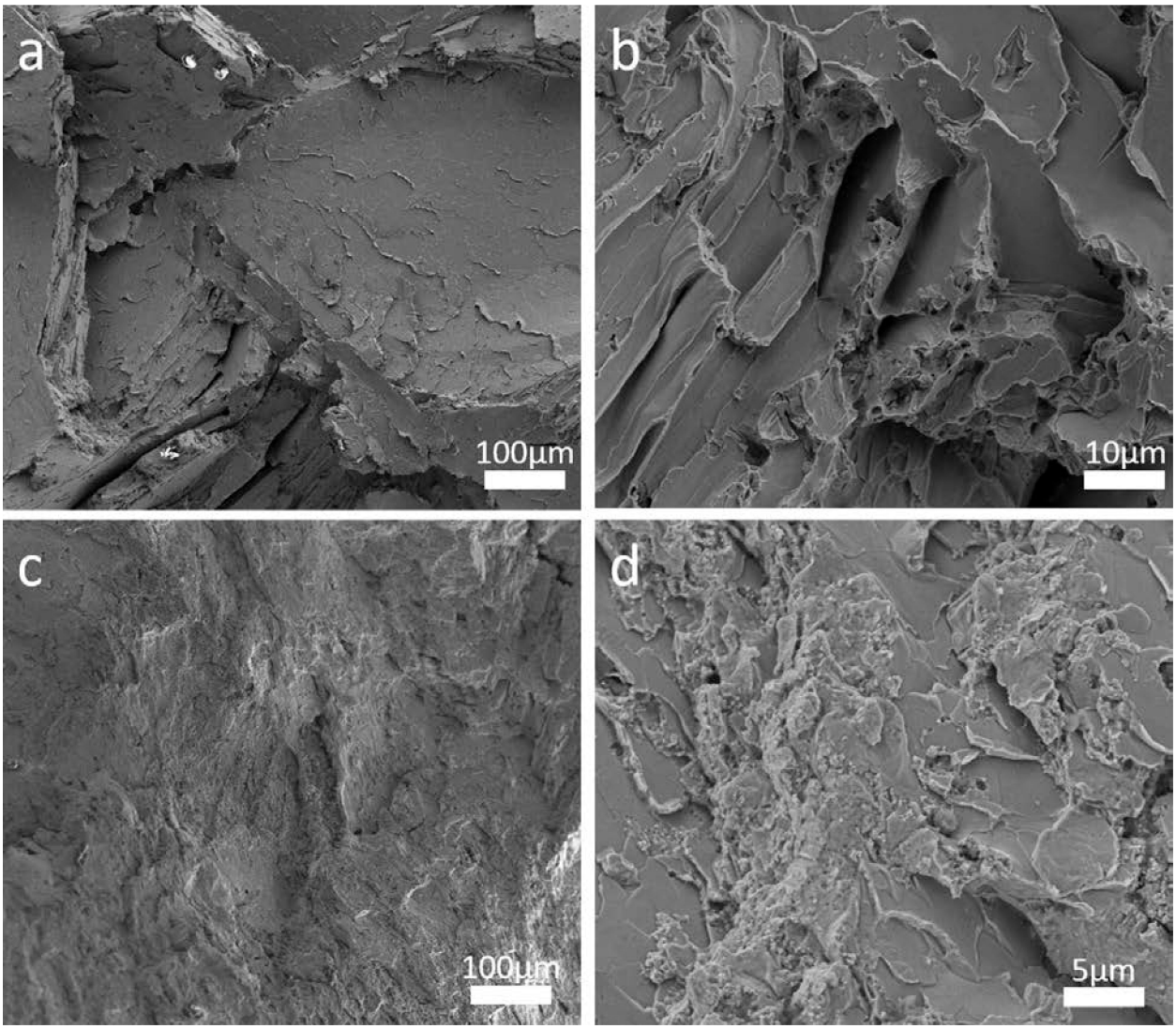

Fig. 8.

The fracture surface of as-cast Zn-2Fe and as-cast Zn-2Fe-WC are shown in (*a*, *b*) and (*c*, *d*), respectively

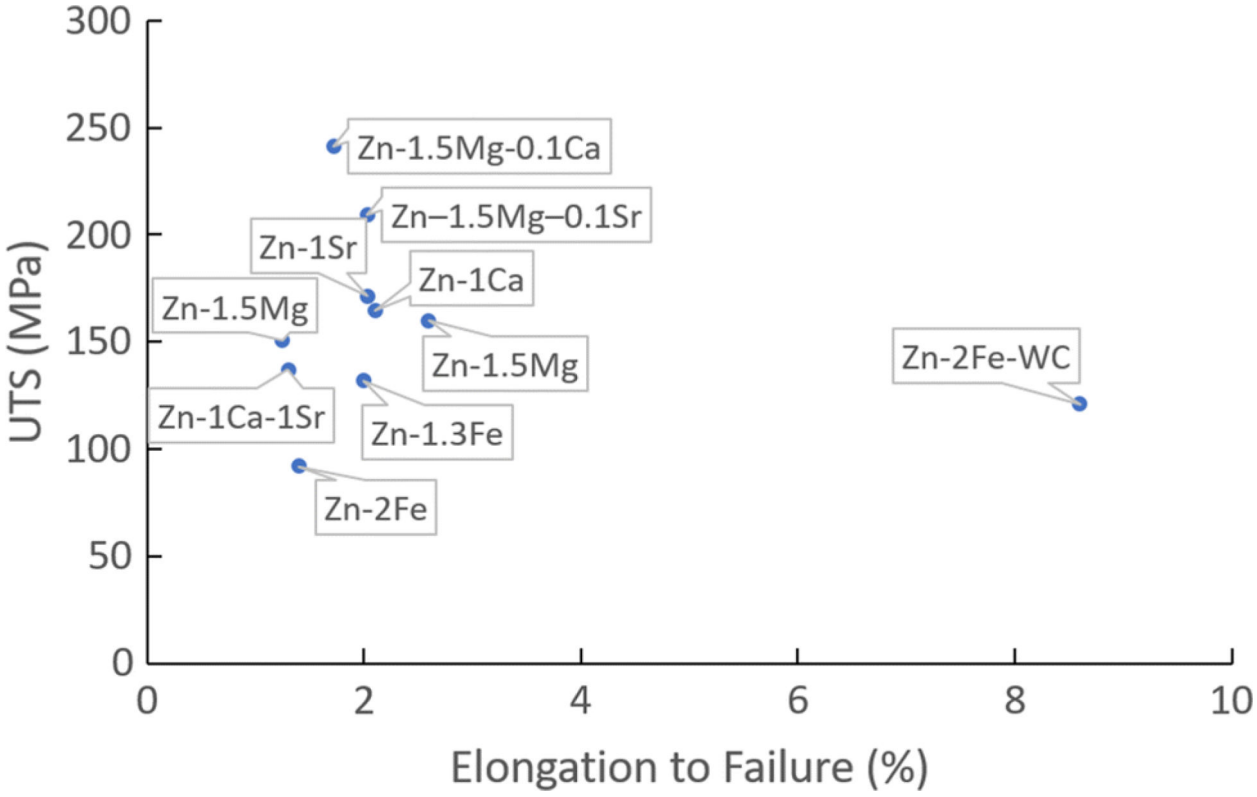

Fig. 9.

UTS vs. elongation to failure for as-cast biocompatible and biodegradable zinc alloys. As-cast Zn-2Fe-WC stands out due to the significantly improved ductility

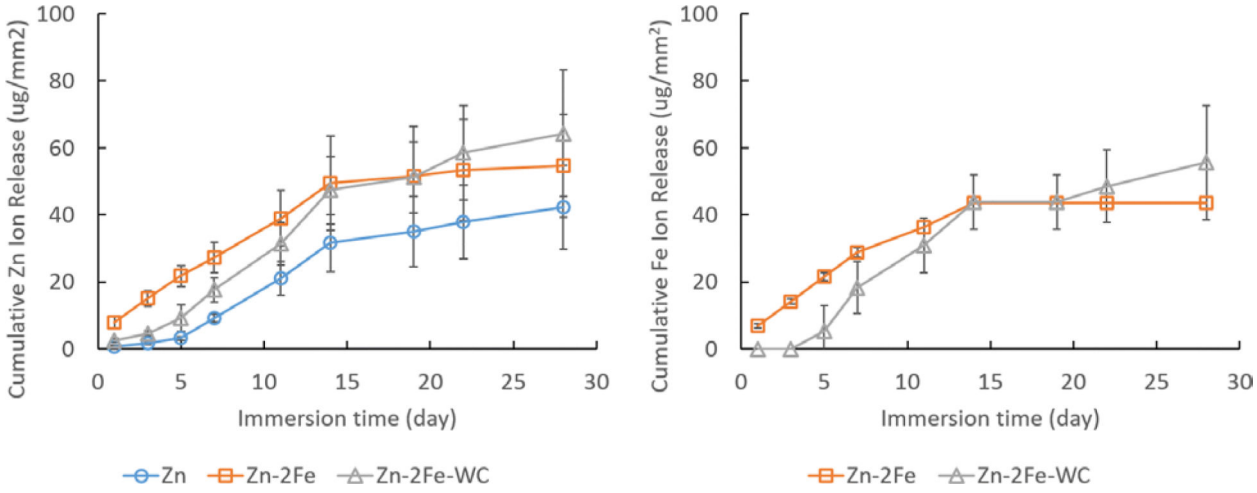

Fig. 10.

Immersion test result: cumulative ion releases of Zn and Fe after 4 weeks in SBF

Table I.

Electrochemical Analysis Data

Sample	Temp (°C)	OCP (V_{SCE})	R_p (kΩ cm^2)	i_{corr} (uA/cm^2)	CR (mm/year)
Zn	37	− 0.966 (± 0.003)	11.978 (± 1.269)	0.81 (± 0.39)	0.012 (± 0.007)
Zn-2Fe	37	− 0.959 (± 0.007)	6.258 (± 0.753)	0.82 (± 0.16)	0.012 (± 0.002)
Zn-2Fe-WC	37	− 0.977 (± 0.022)	5.195 (± 3.383)	1.34 (± 0.50)	0.020 (± 0.007)

OCP open circuit potential, R_p polarization resistance, i_{corr} corrosion current, *C* corrosion rate

Table II.

Cumulative Ion Release at Day 28 ($n = 5$)

Sample	Temp (°C)	Zn (ug/mm^2)	Fe (ug/mm^2)	*W* (ug/mm^2)
Zn	37	42.2 (± 12.5)	N/A	N/A
Zn-2Fe	37	54.6 (± 15.4)	43.6 (± 2.0)	N/A
Zn-2Fe-WC	37	64.3 (± 18.8)	55.6 (± 17.1)	0.002 (± 0.003)